Modeling and Decoupling Control for Rotor System in Magnetic Levitation Wind Turbine

YANJUN YU[1], XIAODONG SUN[2], (Member IEEE), AND WEIYU ZHANG[1]
[1]School of Electrical and Information Engineering, Jiangsu University, Zhenjiang 212013, China
[2]Automotive Engineering Research Institute, Jiangsu University, Zhenjiang 212, China

Corresponding author: Xiaodong Sun (xdsun@ujs.edu.cn)

ABSTRACT This study proposes an accurate mathematical model and a novel decoupling scheme for developing a 5-degrees-of-freedom rotor system of a wind turbine with high robustness, fast response and good-tracking properties. The proposed scheme incorporates neural network generalized inverse (NNGI) control and five model reference adaptive (MRA) controllers. The decoupled open-loop generalized pseudo-linear system can be established by placing the NNGI system in front of the original system. The MRA controllers are utilized to design a closed-loop controller to improve the robustness and anti-disturbance ability of the entire rigid rotor system. The effectiveness of the proposed control scheme is demonstrated via simulation and experimental results for various operations.

INDEX TERMS Wind turbine, decoupling control, neural network generalized inversion, model reference adaptive control, magnetic levitation generator, magnetic bearing.

I. INTRODUCTION

Wind energy is an increasingly important, well-known renewable energy resource and has attracted a large proportion of investments [1], [2]. Manufacturers have replaced the traditional wind turbines with direct-drive wind turbines without gearboxes in recent years because of the high cost and vulnerability of the gearboxes in wind turbines [3], [4]. However, the start-up wind speed of direct-drive wind turbines is higher than that of the traditional wind turbines because of the size and weight of wind turbines. The working conditions of wind turbines, including the heat, high humidity and impact loading, are also poor. Magnetic bearings, which offer efficient shock resistance, long lifetimes, and efficient sealing and lubrication, can be used in direct-drive wind turbines to solve the abovementioned problems [5]–[8].

A magnetic levitation system consists of many magnetic levitation devices, such as magnetic bearings and levitation windings [9]. In addition, the system is a time-varying system that is multivariable, close coupling, and nonlinear. Therefore, the control scheme is complex and difficult to use in a magnetic levitation system. An individual and traditional linear control scheme, i.e., the proportional integral differential (PID), has been used in magnetic levitation systems.

However, the coupling among the system variables is disregarded; thus, many high-performance decoupling control schemes with high accuracy and performance have been used in magnetic levitation systems, such as sliding model control [10], adaptive robust nonlinear control [11], output feedback stepping control [12], and dynamic feedback linearization decoupling [13], [14]. These methods, which were mentioned in previous studies, require an accurate mathematical model, but the accurate mathematical model of a 5-DOF rotor system is difficult to deduce. To solve this problem, neural network inversion has been used in 5-DOF systems [15], [16].

The neural network generalized inverse (NNGI) technology is the improvement of the neural network inverse system method. The NNGI technology can constitute open-loop stable subsystem with the original system in comparison with the neural network inverse system method. Moreover, the obtained subsystem is a linear transfer function of which zeros and poles can be assigned easily, and the integral controllers are also easy to design.

For complex nonlinear systems, the NNGI control scheme can play a role in feedback linearization and multivariable decoupling, and it is simple and easy to understand.

Nevertheless, a few uncertainties are inherent in nonlinear systems because of the modeling error, loading change, and environment [17]–[19]. The model reference adaptive (MRA) controller is used in nonlinear systems, where the tracking signal comes from a set of reference dynamics [20]. Hence, the NNGI control scheme and MRA controllers can be combined in a 5-DOF magnetic levitation system.

The remainder of this paper is organized as follows. The structure and mathematical model of the 5-DOF magnetic levitation direct-drive wind turbine are described in section II. In section III, the NNGI control scheme is used for decoupling of the 5-DOF magnetic levitation system, and the MRA controllers are designed to improve the system robustness. In section IV, simulation and experimental studies are carried out to verify the effectiveness of the proposed control scheme. Finally, the conclusion is given in section V.

II. PRINCIPLES OF GENERALIZED INVERSE AND MRA CONTROLLER

A. BASIC CONCEPT OF GENERALIZED INVERSION

From the viewpoint of functional analysis, a multivariable system Σ can be considered as a mapping θ reflecting the inputs and outputs. Given a system Σ with the inputs $\boldsymbol{u}(t)$, outputs $\boldsymbol{y}(t)$, and the initial vector $\boldsymbol{x}(t_0) = \boldsymbol{x}_0$, the above mapping θ describing the relationship between the inputs and outputs can be defined as follows:

$$\boldsymbol{y}(\cdot) = \boldsymbol{\theta}(\boldsymbol{x}_0, \boldsymbol{u}(\cdot)) \quad \text{or} \quad \boldsymbol{y} = \boldsymbol{\theta}\boldsymbol{u} \tag{1}$$

According to [21] and [22], the definition of the generalized inverse system of mapping θ is as follows:

Definition: Assuming a system Π with p-dimensional input $\boldsymbol{\varphi}(t) = [\varphi_1, \varphi_2, \cdots, \varphi_p]^T$, which is the differential analytic function vector, and q-dimensional output $\boldsymbol{u}_d(t) = [u_{d1}, u_{d2}, \cdots, u_{dq}]^T$, the mapping relation between inputs and outputs is $\boldsymbol{u}_d = \bar{\boldsymbol{\theta}}_g \boldsymbol{\varphi}$, and the inputs and outputs are subject to some initial conditions. Π can be referred to as the generalized inversion of the original system Σ if

$$\boldsymbol{\theta}\bar{\boldsymbol{\theta}}_g\boldsymbol{\varphi} = \boldsymbol{\theta}\boldsymbol{u}_d = \boldsymbol{y}_d \tag{2}$$

where $\boldsymbol{y}_d$ is the expected output vector of Σ, $\boldsymbol{y}_d = [y_{d1}, y_{d2}, \cdots y_{dp}]^T$, and

$$\boldsymbol{\varphi} = a_{i0}y_{di}^{(\alpha)} + a_{i1}y_{di}^{(\alpha-1)} + a_{i2}y_{di}^{(\alpha-2)} + \cdots a_{i\alpha}y_{di},$$
$$i = 1, 2, \cdots, p \tag{3}$$

where $a_{i0}, a_{i1}, \cdots, a_{i\alpha}$ are real numbers and $a_{i0} \neq 0$.

As a MIMO nonlinear system that has q-dimensional input vectors $\boldsymbol{u} = [u_1, u_2, \cdots, u_q]^T \in \boldsymbol{R}^q$ and q-dimensional output vectors $\boldsymbol{y} = [y_1, y_2, \cdots, y_q]^T \in \boldsymbol{R}^q$, the differential equation can be expressed as:

$$\boldsymbol{F}(\boldsymbol{y}^{(\varepsilon)T}, \boldsymbol{Y}, \boldsymbol{u}^{(\sigma)T}, \boldsymbol{U}) = 0 \tag{4}$$

where

$$\varepsilon = (\varepsilon_1, \varepsilon_2, \cdots \varepsilon_q)^T, \quad \sigma = (\sigma_1, \sigma_2, \cdots \sigma_q)^T,$$
$$\boldsymbol{y}^{(\varepsilon)} = (y_1^{(\varepsilon_1)}, \cdots, y_q^{(\varepsilon_q)}), \quad \boldsymbol{u}^{(\sigma)} = (u_1^{(\sigma_1)}, \cdots, u_q^{(\sigma_q)}),$$

$$\boldsymbol{Y} = (y_1^{(\varepsilon_1-1)}, \cdots, y_1, \cdots, y_q^{(\varepsilon_q-1)}, \cdots, y_q)^T,$$
$$\boldsymbol{U} = (u_1^{(\sigma_1)}, \cdots, u_1, \cdots, u_q^{(\sigma_q-1)}, \cdots, u_q)^T,$$

and σ_i and ε_i are the highest derivative orders of input u_i and output y_i, respectively.

According to the theorem in [23], for a MIMO system expressed as in (4) on an open set D, the generalized inversion $\Pi_{\varepsilon\sigma}$ exists, or the system is invertible when $\det[\frac{\partial \boldsymbol{F}}{\partial \boldsymbol{U}^{(M)}}] \neq 0$ and $\frac{\partial \boldsymbol{F}}{\partial \boldsymbol{U}^{(M)}}$ is continuous. The generalized inversion $\Pi_{\varepsilon\sigma}$ is:

$$\begin{cases} \dot{\boldsymbol{z}}_j = \boldsymbol{A}_j\boldsymbol{z}_j + \boldsymbol{B}_j\boldsymbol{v}_j, j \in q \\ \dot{\boldsymbol{o}}_j = \boldsymbol{C}_j\boldsymbol{o}_j + \boldsymbol{D}_j\boldsymbol{e}_j, j \in q \\ \boldsymbol{e} = \phi(\boldsymbol{v}, \boldsymbol{z}, \boldsymbol{o}) \\ \boldsymbol{u} = \boldsymbol{e}^{(-\sigma)} \end{cases} \tag{5}$$

where the output of $\Pi_{\varepsilon\sigma}$ is $\boldsymbol{u} = [u_1, u_2, \cdots, u_q]^T$, the input of $\Pi_{\varepsilon\sigma}$ is $\boldsymbol{v} = (v_1, v_2, \cdots, v_q)^T$, $v_j = y_j^{(\varepsilon_j)}$, $e_j = u_j^{(\sigma_j)} j \in q$, and $(\boldsymbol{A}_j, \boldsymbol{B}_j)$ and $(\boldsymbol{C}_j, \boldsymbol{D}_j)$ are the Brunovsky normalized form matrices of ε_j and σ_j, respectively.

$\boldsymbol{e}^{(-\sigma)} = (e_1^{-\sigma_1}, e_2^{-\sigma_2}, \cdots, e_q^{-\sigma_q})$ is the $\sigma = (\sigma_1, \sigma_2, \cdots, \sigma_q)^T$-order integration of $\boldsymbol{e}$, and the variables and inputs of the system can be expressed as follows:

$$\begin{cases} z_{j(i+1)} = y_j^{(i)}, & j \in q, \ i = 0, 1, \cdots, \varepsilon_j - 1 \\ o_{j(i+1)} = u_j^{(i)}, & j \in q, \ i = 0, 1, \cdots, \sigma_j - 1 \end{cases} \tag{6}$$

$$v_j = \frac{1}{a_{j\varepsilon_j}}[-a_{j0}y_j - -a_{j1}\dot{y}_j - \cdots - a_{j(\varepsilon_j-1)}y_j^{(\varepsilon_j-1)} + \bar{v}_j]$$
$$= \frac{1}{a_{j\varepsilon_j}}[-a_{j0}z_{j1} - -a_{j1}z_{j2} - \cdots - a_{j(\varepsilon_j-1)}z_{j\varepsilon_j} + \bar{v}_j],$$
$$j \in q \tag{7}$$

where $a_{j\varepsilon_j} \neq 0$.

The pseudo-linear composite system can be obtained when the generalized inversion is connected in series with the original system, and the transfer function of inputs and outputs is:

$$G(s)$$
$$= diag(G_{11}(s), \cdots, G_{qq}(s))$$
$$= diag(\frac{1}{a_{1\varepsilon_1}s^{\varepsilon_1} + a_{1(\varepsilon_1-1)}s^{\varepsilon_1-1} + \cdots + a_{11}s + a_{10}}, \cdots,$$
$$\frac{1}{a_{q\varepsilon_q}s^{\varepsilon_q} + a_{q(\varepsilon_q-1)}s^{\varepsilon_q-1} + \cdots + a_{q1}s + a_{q0}}) \tag{8}$$

B. STRUCTURE AND PRINCIPLE OF MRA CONTROLLER

The basic principle of a MRA controller can be summarized as follows: a reference model is designed according to the structure and control requirements of the controlled object, and then the parameters of the controller are adjusted based on the difference between the reference model and the outputs of the controlled object [24], [25]. Finally, the controlled object is made to match up with the characteristics of the ideal reference model. The typical structure of an MRA controller is shown in Fig. 1. The generalized error e is obtained by comparing the reference model with the output of the controlled object, and the functional form of the generalized
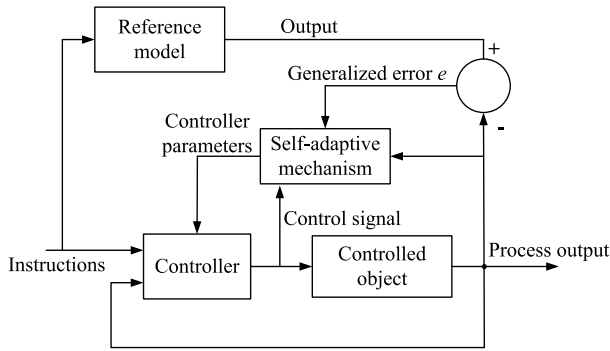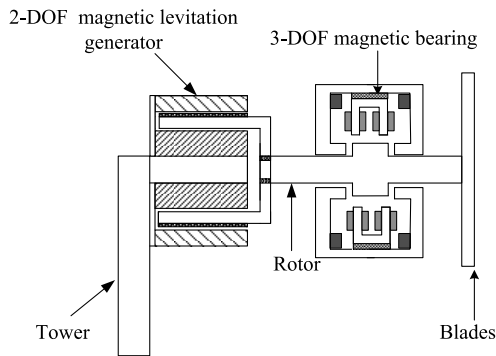
FIGURE 1. Basic structure of MRA controller.

FIGURE 2. Structure of the proposed 5-DOF wind turbine.

FIGURE 3. Cross-section of the 2-DOF generator.
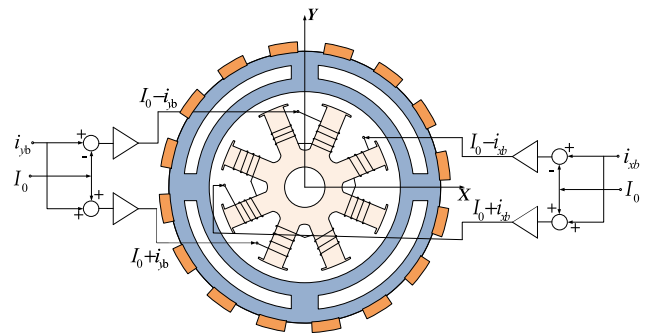
FIGURE 4. Connection diagram of the levitation windings in the inner stator.

error is made to yield a minimum by modifying the controller parameters.

III. STRUCTURE AND MATHEMATICAL MODEL

A. DESCRIPTION OF THE 5-DOF MAGNETIC LEVITATION WIND TURBINE SYSTEM

A novel 5-DOF magnetic levitation wind turbine is proposed in this study, as shown in Fig. 2. The wind turbine consists of a 3-DOF hybrid magnetic bearing with a large carrying capacity and a 2-DOF generator. As for the 5 DOF magnetic levitation wind turbine system, it means that the 2-DOF generator has 2-DOF radial suspension DOF and the 3-DOF hybrid magnetic bearing has 2-DOF radial suspension DOF and single-DOF axial DOF. It's important to note that the 5 DOF magnetic levitation wind turbine system excludes the rotational DOF. The cross-section of the 2-DOF generator, which consists of one inner stator, one outer stator, armature windings, levitation windings, a distributed hollow rotor, and permanent magnets, is shown in Fig. 3. The armature windings are positioned in the outer stator, and the levitation windings are positioned in the inner stator. The surface-mounted permanent magnets adopt a radial magnetization. The coupling between the armature and levitation windings can be relieved by the distributed hollow rotor [26].

As shown in Fig. 3, the magnetic levitation windings are wound around the inner stator poles, and the number of turns of each levitation winding is N_f. The schematic of the
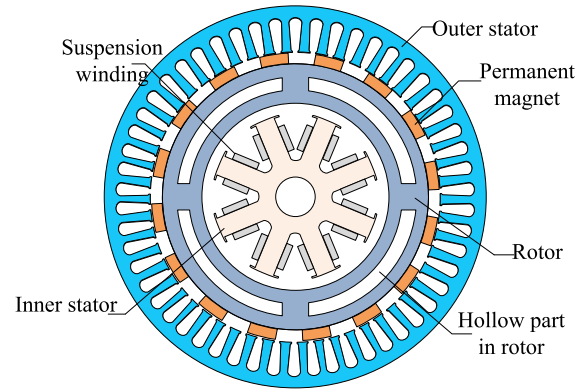
connection and control method is shown in Fig. 4. Every two adjacent windings are connected in series, and the differential controllers are used in the radial direction. The principle of levitation force generation is that the current i_{xb} will be added to the circuit when the rotor is shifted off the equilibrium position to the left side. According to the principle of Maxwell force generation, the rotor will be pulled back by the levitation force because of the difference current in the levitation windings. The principle of levitation force on the other side is the same as that presented above.
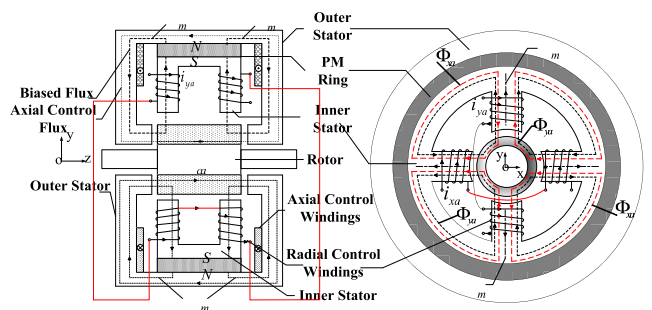

FIGURE 5. Structure of the 3-DOF hybrid magnetic bearing.

The structure of the 3-DOF hybrid magnetic bearing and the connection with the levitation windings are shown in Fig. 5. The bearing consists of one outer stator, one inner

stator with eight poles, a radial magnetized permanent magnet ring, axial levitation windings, radial levitation windings, and a rotor. The eight poles are set in the inner stator to increase the carrying capacity and tolerance of the hybrid magnetic bearing. Bias flux is provided by the permanent magnet ring in this magnetic bearing.

The working principle of the 3-DOF magnetic bearing is that the radial control current i_{ya} is loaded when the rotor is shifted off the equilibrium position toward the negative direction of the y-axis; then, the magnitude of the upper air gap flux is greater than that of the lower air gap flux because the flux Φ_{ya} generated by i_{ya} is superimposed with the bias flux Φ_m in the upper air gap and offsetting occurs between Φ_{ya} and Φ_m in the lower air gap. According to the principle of Maxwell force generation, the rotor will be pulled back to the equilibrium position because a difference force is applied to the rotor. The principle of the levitation force in the other directions is the same; the z-axis control flux is Φ_{ca}, and the x-axis control flux is Φ_{xa}.

In conclusion, the rigid rotor of the wind turbine system can be suspended by the 2-DOF magnetic levitation generator on the left side and by the 3-DOF magnetic bearing on the right side. The forces acting on the rigid rotor are depicted in Fig. 6. The forces F_{yb} and F_{xb} on the left side are produced by the 2-DOF magnetic levitation generator, and F_{ya}, F_{xa} and F_z on the right side are produced by the 3-DOF magnetic bearing. F_{dx}, F_{dy}, and F_{dz} are the disturbances from the load or environment; O is the centroid of the rigid rotor; and mg is the weight of the rotor.

B. MODELING OF LEVITATION FORCES IN 2-DOF MAGNETIC LEVITATION GENERATOR

The modeling of the 3-DOF magnetic bearing and the 2-DOF generator can be deduced because the 5-DOF magnetic levitation wind turbine system is suspended by two different structures. The following assumptions are made to simplify the magnetic circulation:

(1) The reluctance of the stator iron core and the rotor core is not considered.
(2) Finite coercivities and magnetic saturation are ignored.
(3) The influence of the compensating current is disregarded.

The principle of virtual displacement indicates that the electromagnetic force suffered by a rotor is equal to the partial derivatives of magnetic energy storage W_a, i.e.,

$$W_a = \frac{1}{2}BHV = \frac{1}{2}BHAl \tag{9}$$

where B is the flux density of the air gap, H is the magnetic field intensity, V is the volume of the air gap under the two levitation poles, l is the length of the air gap, and A is the cross-section of the levitation pole. The electromagnetic force suffered by the rotor under the levitation pole is

$$f = \frac{\partial W_a}{\partial l} = \frac{1}{2}BHA = \frac{B^2A}{2\mu_0} \tag{10}$$
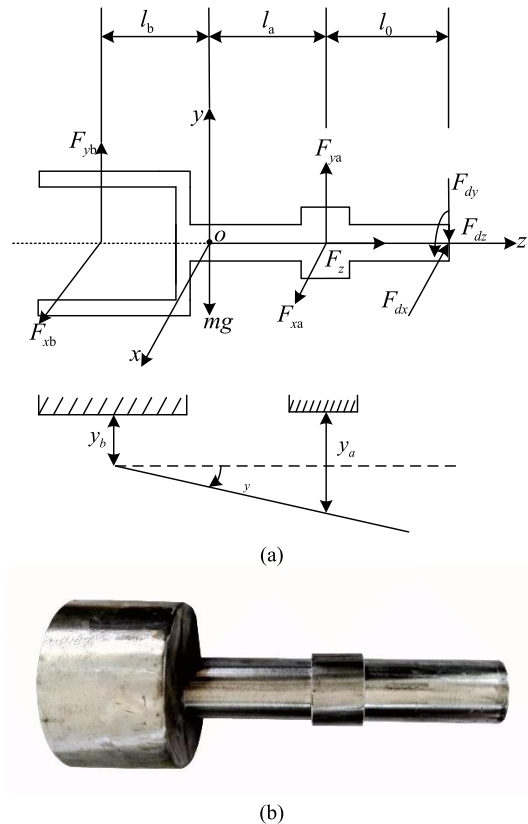

FIGURE 6. Rigid rotor of the wind turbine system. (a) Forces acting on the rigid rotor. (b) Photograph of the rigid rotor.

According to Ampere's law, the flux density is assumed to remain constant, i.e.,

$$B = \mu_0 \frac{Ni}{l} \tag{11}$$

By combining (10) and (11), we obtain

$$f = k\frac{i^2}{l^2} \tag{12}$$

where Ni is the magnetomotive force, $\mu_0 = 4\pi \times 10^{-7}$ H/m, and $k = \frac{\mu_0 N^2 A}{2}$.

There are eight levitation forces acting on the hollow rotor in the 2-DOF magnetic levitation generator. Considering that the angle among the forces is $\alpha = 22.5°$, the composition of every two radial levitation forces along the radial axis is

$$f = 2 \times k\frac{i^2}{l^2}\cos 22.5° \tag{13}$$

Then, the radial levitation forces acting on the rotor on the left side are

$$F_{xb} = 2\cos 22.5°k[\frac{(I_0 + i_{xb})^2}{x_b^2} - \frac{(I_0 - i_{xb})^2}{(2g_0 - x_b)^2}] \tag{14}$$

$$F_{yb} = 2\cos 22.5°k[\frac{(I_0 + i_{yb})^2}{y_b^2} - \frac{(I_0 - i_{yb})^2}{(2g_0 - y_b)^2}] \tag{15}$$

$$F_{xa} = 4g_0 S_r \mu_0 \{ \frac{1}{\sigma_a} \cdot \frac{y_a S_z F_m (2g_0 - y_a)}{x_a y_a S_z (2g_0 - x_a)(2g_0 - y_a) + 2g_0 z S_r (2g_0 y_a - y_a^2 + 2g_0 x_a - x_a^2)}$$

$$+ \frac{n_{xa} i_{xa}}{\sigma_c} [\frac{1}{y_a (2g_0 - y_a) + 2g_0 x_a} - \frac{1}{y_a (2g_0 - y_a) + 2g_0 (2g_0 - x_a)}]$$

$$\times \{ \frac{1}{\sigma_a} \cdot \frac{y_a S_z F_m (2g_0 - y_a)(g_0 - x_a)}{x_a y_a S_z (2g_0 - x_a)(2g_0 - y_a) + 2g_0 z S_r (2g_0 y_a - y_a^2 + 2g_0 x_a - x_a^2)}$$

$$+ \frac{g_0 n_{xa} i_{xa}}{\sigma_c} [\frac{1}{y_a (2g_0 - y_a) + 2g_0 x_a} + \frac{1}{y_a (2g_0 - y_a) + 2g_0 (2g_0 - x_a)}] \} \} \tag{19}$$

$$F_{ya} = 4g_0 S_r \mu_0 \{ \frac{1}{\sigma_a} \cdot \frac{x_a S_z F_m (2g_0 - x_a)}{x_a y_a S_z (2g_0 - x_a)(2g_0 - y_a) + 2g_0 z S_r (2g_0 y_a - y_a^2 + 2g_0 x_a - x_a^2)}$$

$$+ \frac{n_{ya} i_{ya}}{\sigma_c} [\frac{1}{x_a (2g_0 - x_a) + 2g_0 y_a} - \frac{1}{x_a (2g_0 - x_a) + 2g_0 (2g_0 - y_a)}] \}$$

$$\times \{ \frac{1}{\sigma_a} \cdot \frac{x_a S_z F_m (2g_0 - x_a)(g_0 - y_a)}{x_a y_a S_z (2g_0 - x_a)(2g_0 - y_a) + 2g_0 z S_r (2g_0 y_a - y_a^2 + 2g_0 x_a - x_a^2)}$$

$$+ \frac{g_0 n_{ya} i_{ya}}{\sigma_c} [\frac{1}{x_a (2g_0 - x_a) + 2g_0 y_a} + \frac{1}{x_a (2g_0 - x_a) + 2g_0 (2g_0 - y_a)}] \} \} \tag{20}$$

where g_0 is the air gap width when the rotor is at the equilibrium position; I_0 is the bias current in the control circuit; i_{xb} and i_{yb} are the control currents of the generator in the x and y directions, respectively; and x_b and y_b are the real air gap lengths between the rotor and inner stator on the left side.

On the basis of Taylor expansion and by omitting the high-order items, (14) and (15) are transformed as follows

$$\begin{cases} F_{xb} \approx k_{ib} \cdot i_{xb} + k_{xyb} \cdot (x_b - g_0) \\ F_{yb} \approx k_{ib} \cdot i_{yb} + k_{xyb} \cdot (y_b - g_0) \end{cases} \tag{16}$$

where $k_{ib} = \frac{8kI_0 \cdot \cos 22.5°}{g_0^2}$ and $k_{xyb} = -\frac{8kI_0^2 \cdot \cos 22.5°}{g_0^3}$.

C. MODELING OF THE 3-DOF MAGNETIC BEARING

As shown in Figs. 5 and 6, and according to (10), the radial electromagnetic forces produced by the magnetic bearing on the rotor on the right side can be expressed as follows

$$F_{xa} = 2 (\frac{B_{x1a}^2 S_r}{2\mu_0} - \frac{B_{x2a}^2 S_r}{2\mu_0}) \tag{17}$$

$$F_{ya} = 2 (\frac{B_{y1a}^2 S_r}{2\mu_0} - \frac{B_{y2a}^2 S_r}{2\mu_0}) \tag{18}$$

where S_r is the cross-sectional area of the tooth of the inner stator and B_{x1a}, B_{x2a}, B_{y1a}, and B_{y2a} are the air gap flux densities in the radial x and y directions. The parameters of the magnetic bearing can be substituted into (17) and (18) as well as (19) and (20), as shown at the top of this page, where i_{xa} and i_{ya} are the control currents of the magnetic bearings in the radial direction; x_a and y_a are the real air gap lengths between the rotor and inner stator on the right side; n_{xa} and n_{ya} are the numbers of turns in the x and y directions, respectively; S_z is the cross-sectional area of the poles in the z-direction; σ_a and σ_c are the correction factors of the radial and axial control

magnetic circuits, respectively; and F_m is the magnetomotive force source of the permanent magnet ring.

In accordance with Taylor expansion and by omitting the high-order items, (19) and (20) are converted into

$$\begin{cases} F_{xa} \approx k_{xai} \cdot i_{xa} + k_{xya} \cdot (x_a - g_0) \\ F_{ya} \approx k_{yai} \cdot i_{ya} + k_{xya} \cdot (y_a - g_0) \end{cases} \tag{21}$$

where $k_{xai} = \frac{8 S_r S_z \mu_0 F_m n_{xa}}{3\sigma_a \sigma_c g_0^2 (4S_r + S_z)}$, $k_{yai} = \frac{8 S_r S_z \mu_0 F_m n_{ya}}{3\sigma_a \sigma_c g_0^2 (4S_r + S_z)}$, and $k_{xya} = -\frac{4 S_r S_z^2 F_m^2 \mu_0}{\sigma_a^2 g_0^3 (4S_r + S_z)^2}$.

The axial electromagnetic forces produced by the magnetic bearing on the rotor can be expressed as

$$F_z = \{ \frac{y_a S_r S_z F_m (x_a + y_a + 2g_0)}{2\sigma_a} \times [\frac{1}{S_z g_0^2 + 2z S_r (x_a + y_a)}$$

$$+ \frac{1}{S_z g_0^2 + 2(2g_0 - z) S_r (x_a + y_a)}] \}$$

$$\times \{ \frac{\mu_0 y_a S_r F_m (x_a + y_a + 2g_0)}{\sigma_a} \times [\frac{1}{S_z g_0^2 + 2z S_r (x_a + y_a)}$$

$$- \frac{1}{S_z g_0^2 + 2(2g_0 - z) S_r (x_a + y_a)}] + \frac{2\mu_0 n_z i_z}{\sigma_c g_0} \} \tag{22}$$

where z is the real air gap length between the rotor and outer stator in the axial direction.

On the basis of Taylor expansion and by omitting the high-order items, (22) is expressed as:

$$F_z \approx k_{zi} \cdot i_z + k_z \cdot (z - g_0) \tag{23}$$

where $k_{zi} = \frac{16 F_m S_r S_z \mu_0 n_z}{\sigma_a \sigma_c g_0 (4S_r + S_z)}$ and $k_z = -\frac{256 \mu_0 F_m^2 S_r^3 S_z}{\sigma_a^2 g_0 (S_z + 4S_r)^3}$.

D. MATHEMATICAL MODEL OF 5-DOF ROTOR SYSTEM

According to the rotor dynamics theory and Newton's second law, the dynamic model of the 5-DOF rotor system equations

can be expressed as follows

$$
\begin{cases}
m\ddot{x} = F_{xa} + F_{xb} - F_{dx} \\
m\ddot{y} = F_{ya} + F_{yb} - F_{dy} - mg \\
m\ddot{z} = F_z - F_{dz} \\
J\ddot{\theta}_x - J_z\omega\dot{\theta}_y = F_{xb}l_b - F_{xa}l_a + F_{dx}(l_a + l_0) \\
J\ddot{\theta}_y + J_z\omega\dot{\theta}_x = -F_{yb}l_b + F_{ya}l_a + F_{dy}(l_a + l_0)
\end{cases}
\tag{24}
$$

$$
\begin{cases}
\theta_x = \dfrac{1}{l_a + l_b}(x_a - x_b) \\
\theta_y = \dfrac{1}{l_a + l_b}(y_a - y_b) \\
x = \dfrac{l_b}{l_a + l_b}x_a + \dfrac{l_a}{l_a + l_b}x_b \\
y = \dfrac{l_b}{l_a + l_b}y_a + \dfrac{l_a}{l_a + l_b}y_b
\end{cases}
\tag{25}
$$

where x, y, and z are the displacements of the centroid in the x-, y-, and z-directions, respectively; J is the moment of inertia of the rotor in the x- and y-directions; J_z is the moment of inertia of the rotor in the z-direction; and θ_x and θ_y are the rotation angles of the rotor relative to the XZ and YZ planes, respectively.

(16), (21), (23), and (25) are substituted into (24), i.e.,

$$
\begin{cases}
\ddot{x}_a = \dfrac{J - ml_a^2}{mJ}[k_{xai}i_{xa} + k_{xya}(x_a - g_0)] + \dfrac{J_zl_a\omega(\dot{y}_a - \dot{y}_b)}{J(l_a + l_b)} \\
\quad + \dfrac{J + ml_al_b}{mJ}[k_{ib}i_{xb} + k_{xyb}(x_b - g_0)] \\
\quad + \dfrac{ml_a(l_a + l_0) - J}{mJ}F_{dx} \\
\ddot{x}_b = \dfrac{J + ml_al_b}{mJ}[k_{xai}i_{xa} + k_{xya}(x_a - g_0)] \\
\quad - \dfrac{J_zl_b\omega(\dot{y}_a - \dot{y}_b)}{J(l_a + l_b)} + \dfrac{J - ml_b^2}{mJ}[k_{ib}i_{xb} + k_{xyb}(x_b - g_0)] \\
\quad - \dfrac{J + ml_b(l_a + l_0)}{mJ}F_{dx} \\
\ddot{y}_a = \dfrac{J + ml_a^2}{mJ}[k_{yai}i_{ya} + k_{xya}(y_a - g_0)] \\
\quad - \dfrac{J_zl_a\omega(\dot{x}_a - \dot{x}_b)}{J(l_a + l_b)} + \dfrac{J - ml_al_b}{mJ} \\
\quad \times [k_{ib}i_{yb} + k_{xyb}(y_b - g_0)] \\
\quad + \dfrac{ml_a(l_a + l_0) - J}{mJ}F_{dy} - g \\
\ddot{y}_b = \dfrac{J - ml_al_b}{mJ}[k_{yai}i_{ya} + k_{xya}(y_a - g_0)] \\
\quad + \dfrac{J_zl_b\omega(\dot{x}_a - \dot{x}_b)}{J(l_a + l_b)} + \dfrac{J + ml_b^2}{mJ}[k_{ib}i_{yb} + k_{xyb}(y_b - g_0)] \\
\quad - \dfrac{J + ml_b(l_a + l_0)}{mJ}F_{dy} - g \\
\ddot{z} = \dfrac{k_{zi}}{m}i_z + \dfrac{k_z}{m}(z - g_0) - \dfrac{F_{dz}}{m}
\end{cases}
\tag{26}
$$

As seen from (26), there are some couplings in the rotor system. For instance, the displacements in the x-direction will be affected by the displacements in the y-direction, and

the flux in the air gap will be changed with arbitrary displacements. Therefore, it is necessary to apply the decoupling method to the rotor system.

E. ANALYSIS OF INVERTIBILITY OF 5-DOF MAGNETIC LEVITATION WIND TURBINE SYSTEM

(26) shows that five input and output variables exist in the 5-DOF rotor system. The input variables U, the output variables Y, and the state variables X can be defined as follows

$$
U = [u_1, u_2, u_3, u_4, u_5]^T = [i_{xa}, i_{xb}, i_{ya}, i_{yb}, i_z]^T \tag{27}
$$

$$
Y = [y_1, y_2, y_3, y_4, y_5]^T = [x_a, x_b, y_a, y_b, z]^T \tag{28}
$$

$$
\begin{aligned}
X &= [x_1, x_2, x_3, x_4, x_5, x_6, x_7, x_8, x_9, x_{10}]^T \\
&= [x_a, x_b, y_a, y_b, z, \dot{x}_a, \dot{x}_b, \dot{y}_a, \dot{y}_b, \dot{z}]^T
\end{aligned}
\tag{29}
$$

(26) can be rewritten as

$$
\begin{cases}
\dot{x}_1 = x_6 \\
\dot{x}_2 = x_7 \\
\dot{x}_3 = x_8 \\
\dot{x}_4 = x_9 \\
\dot{x}_5 = x_{10}
\end{cases}
\tag{30}
$$

$$
\begin{cases}
\dot{x}_6 = \dfrac{J - ml_a^2}{mJ}[k_{xai}u_1 + k_{xya}(x_1 - g_0)] \\
\quad + \dfrac{J_zl_a\omega(x_8 - x_9)}{J(l_a + l_b)} + \dfrac{J + ml_al_b}{mJ} \\
\quad \times [k_{ib}u_2 + k_{xyb}(x_2 - g_0)] + \dfrac{ml_a(l_a + l_0) - J}{mJ}F_{dx} \\
\dot{x}_7 = \dfrac{J + ml_al_b}{mJ}[k_{xai}u_1 + k_{xya}(x_1 - g_0)] \\
\quad - \dfrac{J_zl_b\omega(x_8 - x_9)}{J(l_a + l_b)} + \dfrac{J - ml_b^2}{mJ} \\
\quad \times [k_{ib}u_2 + k_{xyb}(x_2 - g_0)] - \dfrac{J + ml_b(l_a + l_0)}{mJ}F_{dx} \\
\dot{x}_8 = \dfrac{J + ml_a^2}{mJ}[k_{yai}u_3 + k_{xya}(x_3 - g_0)] \\
\quad - \dfrac{J_zl_a\omega(x_6 - x_7)}{J(l_a + l_b)} + \dfrac{J - ml_al_b}{mJ} \\
\quad \times [k_{ib}u_4 + k_{xyb}(x_4 - g_0)] + \dfrac{ml_a(l_a + l_0) - J}{mJ}F_{dy} - g \\
\dot{x}_9 = \dfrac{J - ml_al_b}{mJ}[k_{yai}u_3 + k_{xya}(x_3 - g_0)] \\
\quad + \dfrac{J_zl_b\omega(x_6 - x_7)}{J(l_a + l_b)} + \dfrac{J + ml_b^2}{mJ} \\
\quad \times [k_{ib}u_4 + k_{xyb}(x_4 - g_0)] - \dfrac{J + ml_b(l_a + l_0)}{mJ}F_{dy} - g \\
\dot{x}_{10} = \dfrac{k_{zi}}{m}u_5 + \dfrac{k_z}{m}(x_5 - g_0) - \dfrac{F_{dz}}{m}
\end{cases}
\tag{31}
$$

The invertibility of the system should be analyzed to construct the inverse system of the rotor system. According to the inverse system theory and using the interactor algorithm, the outputs of the 5-DOF system are differentiated until the

derivatives contain input U.

$$\mathbf{Y}_5 = \begin{bmatrix} y_1^{(\alpha_1)} \\ y_2^{(\alpha_2)} \\ y_3^{(\alpha_3)} \\ y_4^{(\alpha_4)} \\ y_5^{(\alpha_5)} \end{bmatrix}$$

$$= \begin{bmatrix} \frac{J - ml_a^2}{mJ}[k_{xai}u_1 + k_{xya}(x_1 - g_0)] \\ + \frac{J_z l_a \omega(x_8 - x_9)}{J(l_a + l_b)} + \frac{J + ml_a l_b}{mJ} \\ \times [k_{ib}u_2 + k_{xyb}(x_2 - g_0)] + \frac{ml_a(l_a + l_0) - J}{mJ}F_{dx} \\[6pt] \frac{J + ml_a l_b}{mJ}[k_{xai}u_1 + k_{xya}(x_1 - g_0)] \\ - \frac{J_z l_b \omega(x_8 - x_9)}{J(l_a + l_b)} + \frac{J - ml_b^2}{mJ} \\ \times [k_{ib}u_2 + k_{xyb}(x_2 - g_0)] - \frac{J + ml_b(l_a + l_0)}{mJ}F_{dx} \\[6pt] \frac{J + ml_a^2}{mJ}[k_{yai}u_3 + k_{xya}(x_3 - g_0)] \\ - \frac{J_z l_a \omega(x_6 - x_7)}{J(l_a + l_b)} + \frac{J - ml_a l_b}{mJ} \\ \times [k_{ib}u_4 + k_{xyb}(x_4 - g_0)] + \frac{ml_a(l_a + l_0) - J}{mJ}F_{dy} - g \\[6pt] \frac{J - ml_a l_b}{mJ}[k_{yai}u_3 + k_{xya}(x_3 - g_0)] \\ + \frac{J_z l_b \omega(x_6 - x_7)}{J(l_a + l_b)} + \frac{J + ml_b^2}{mJ} \\ \times [k_{ib}u_4 + k_{xyb}(x_4 - g_0)] - \frac{J + ml_b(l_a + l_0)}{mJ}F_{dy} - g \\[6pt] \frac{k_{zi}}{m}u_5 + \frac{k_z}{m}(x_5 - g_0) - \frac{F_{dz}}{m} \end{bmatrix} \tag{32}$$

where $\alpha_1 = \alpha_2 = \alpha_3 = \alpha_4 = \alpha_5 = 2$.

The Jacobi matrix can be derived as (33), as shown at the bottom of this page.

The coefficients k_{xai}, k_{ib}, k_{yai}, and k_{zi} will not be zero when the structure and parameters of the rotor system are established. Thus, $\det[\frac{\partial \mathbf{Y}_5}{\partial \mathbf{u}^T}] \neq 0$, and (33) is nonsingular.

FIGURE 7. Diagram of the generalized pseudo-linear system.

The relative order of the rotor system α is

$$\alpha = n_e = [\alpha_1 = \alpha_2 = \alpha_3 = \alpha_4 = \alpha_5] = [2 \quad 2 \quad 2 \quad 2 \quad 2]^T \tag{34}$$

where n_e is the essential order of the system. The generalized inversion of the original system is therefore existent.

The linear system is now introduced to establish the stable pseudo-linear system according to the generalized inverse theory [26]. The inputs of the 5-DOF rotor system can be given as

$$u = \phi[(\dot{y}_1, y_1, \dot{y}_2, y_2, \dot{y}_3, y_3, \dot{y}_4, y_4, \dot{y}_5, y_5), \hat{v}] \tag{35}$$

$$\hat{v} = [\hat{v}_1, \hat{v}_2, \hat{v}_3, \hat{v}_4, \hat{v}_5]^T \tag{36}$$

$$\begin{cases} \hat{v}_1 = a_{12}\ddot{y}_1 + a_{11}\dot{y}_1 + a_{10}y_1 \\ \hat{v}_2 = a_{22}\ddot{y}_2 + a_{21}\dot{y}_2 + a_{20}y_2 \\ \hat{v}_3 = a_{32}\ddot{y}_3 + a_{31}\dot{y}_3 + a_{30}y_3 \\ \hat{v}_4 = a_{42}\ddot{y}_4 + a_{41}\dot{y}_4 + a_{40}y_4 \\ \hat{v}_5 = a_{52}\ddot{y}_5 + a_{51}\dot{y}_5 + a_{50}y_5 \end{cases} \tag{37}$$

where a_{ij} ($i = 1, 2, 3, 4, 5; j = 0, 1, 2$) is the pole assignment coefficient. (35) can be considered as being in series with the original system; thus, the generalized pseudo-linear system is

$$\mathbf{G}(s) = diag(G_{11}(s), G_{22}(s), G_{33}(s), G_{44}(s), G_{55}(s))$$

$$= diag(\frac{1}{a_{12}s^2 + a_{11}s + a_{10}}, \frac{1}{a_{22}s^2 + a_{21}s + a_{20}},$$

$$\frac{1}{a_{32}s^2 + a_{31}s + a_{30}}, \frac{1}{a_{42}s^2 + a_{41}s + a_{40}},$$

$$\frac{1}{a_{52}s^2 + a_{51}s + a_{50}}) \tag{38}$$

$$\frac{\partial \mathbf{Y}_5}{\partial \mathbf{u}^T} = \begin{bmatrix} \frac{J - ml_a^2}{mJ}k_{xai} & \frac{J + ml_a l_b}{mJ}k_{ib} & 0 & 0 & 0 \\ \frac{J + ml_a l_b}{mJ}k_{xai} & \frac{J - ml_b^2}{mJ}k_{ib} & 0 & 0 & 0 \\ 0 & 0 & \frac{J + ml_a^2}{mJ}k_{yai} & \frac{J - ml_a l_b}{mJ}k_{ib} & 0 \\ 0 & 0 & \frac{J - ml_a l_b}{mJ}k_{yai} & \frac{J + ml_b^2}{mJ}k_{ib} & 0 \\ 0 & 0 & 0 & 0 & \frac{k_{zi}}{m} \end{bmatrix} \tag{33}$$
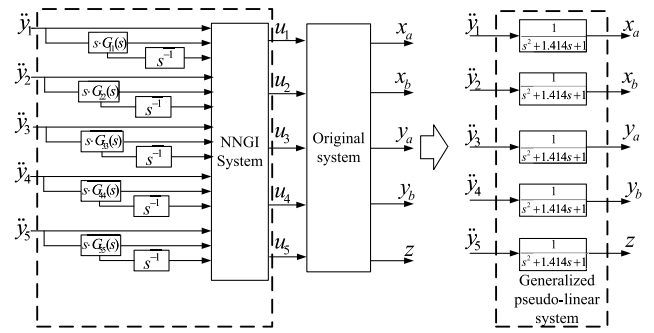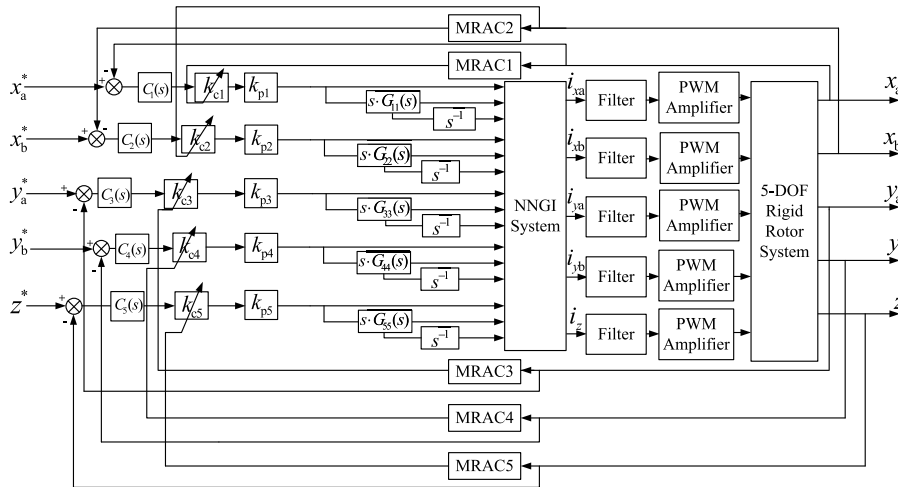
FIGURE 8. Control block diagram of the entire system.

The coefficients are selected to be $a_{12} = a_{22} = a_{32} = a_{42} = a_{52} = 1$, $a_{11} = a_{21} = a_{31} = a_{41} = a_{51} = 1.414$, and $a_{10} = a_{20} = a_{30} = a_{40} = a_{50} = 1$ to construct an optimal second-order system.

IV. MRA CONTROLLER-BASED NNGI CONTROL STRATEGY

The neural network, which has a strong nonlinear approximation capability, can be used to construct the generalized inversion of the 5-DOF wind turbine because of the uncertainties of the mathematical model deduced in the previous section. The feedback closed-loop control system with the MRA controller must be used in the NNGI system of the 5-DOF wind turbine to achieve high robustness.

A. NNGI SYSTEM

The process of realizing the NNGI system includes determination and training of the NNGI system. The arithmetic results from the mathematical expression of the generalized inverse system are introduced into the neural network to increase the adaptability and anti-disturbance of the generalized inversion. The back propagation (BP) neural network is utilized in the generalized inversion of the 5-DOF rotor system, and five integrators and five differentiators are used to characterize the dynamic characteristics. The five-point numerical differential algorithm is used in this study. The inputs and outputs of the neural network are $\{x_a, \dot{x}_a, \ddot{x}_a, x_b, \dot{x}_b, \ddot{x}_b, y_a, \dot{y}_a, \ddot{y}_a, y_b, \dot{y}_b, \ddot{y}_b, z, \dot{z}, \ddot{z}\}$ and $\{x_a, x_b, y_a, y_b, z\}$. According to the inputs and outputs of the BP neural network, the numbers of neurons in the input, hidden, and output layers are set as 15, 30, and 5, respectively.

The trained BP neural network can be considered as in series with the original system. A generalized pseudo-linear system can be built, as illustrated in Fig. 7. Fig. 7 shows that the generalized pseudo-linear system is equivalent to five independent second-order linear integral subsystems, and an

accurate model of the original system is not needed in this developed scheme.

B. 5-DOF MRA CONTROLLERS

As shown in Fig. 7, the original system can be decoupled by cascading the NNGI system with the original system. A simple open-loop system, which is more affected by many factors in practical application, is then obtained. The closed-loop controllers are essential in this study to improve the system performance.

The MRA controllers are used in the closed-loop system to increase the robustness. The control block diagram of the proposed 5-DOF wind turbine based on the NNGI control scheme and MRA controllers is shown in Fig. 8.
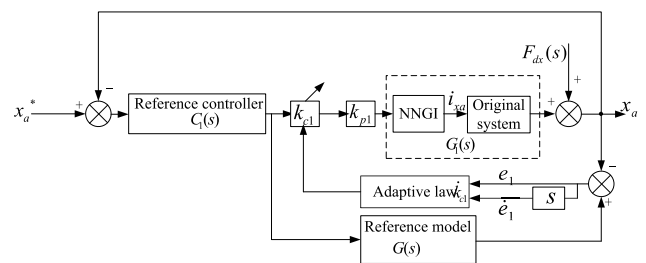

FIGURE 9. Closed-loop system of the MRA controller in the x_a-direction.

As shown in Fig. 8, the 5-DOF rotor system controller can be designed according to the control theory of linear systems because five displacements are decoupled. The controllers for the five subsystems can then be designed independently. The adaptive law for every single-input and single-output system can be deduced when the reference model is set as $G(s) = 1/s^2 + 1.414s + 1$. The x_a-direction radial displacement is taken as an example, and the structure of MRA1 and the control schematic program in the x_a-direction are shown in Fig. 9. In the figure, x_a* and x_a are the given input and actual output in the x_a-direction, respectively; $G_1(s)$ is the

TABLE 1. Parameters of the 5-DOF rigid rotor system.

Parameter	Value	Parameter	Value
m	13 kg	k_{xai}	101 N/A
J_x	0.04035 kg·m^2	k_{yai}	95 N/A
J_y	0.04035 kg·m^2	k_{xya}	10100 N/m
J_y	0.12 kg·m^2	k_{zi}	305 N/A
l_a	0.505 m	k_z	-4600 N/m
l_b	0.65 m	k_{ib}	406 N/A
L_0	0.45 m	k_{xyb}	-55000 N/m

generalized pseudo-linear system in the x_a-direction; $G(s)$ is the reference model in the x_a-direction; $F_{dx}(s)$ is the perturbation in the x_a-direction; k_{p1} is the actual gain; k_{c1} is the adjustable gain; $C_1(s)$ is the reference controller in the x_a-direction; and e_1 and $\dot{e}_1$ are the error and the rate of change error, respectively. Therefore, in the wind power generation process, by using the proposed control scheme, the multivariable, non-linear, and coupled original system is equivalent to five independent second-order linear integral subsystems. Since the robustness and anti-disturbance properties of the 5-DOF suspension control is improved greatly, the whole performance of the 5 DOF magnetic levitation wind turbine system, such as energy capture, can be significantly enhanced as well. Thereby, more realistic future research will benefit from focusing on optimization of wind power generation in some typical operation conditions.

The closed-loop transfer function of the subsystem in the x_a-direction is

$$\phi_1(s) = G(s) - G_1(s) = k_1/(s^2 + 1.414s + 1) \quad (39)$$

where $k_1 = 1 - k_{c1}k_{p1}$.

The adaptive law in the x_a-direction can be deduced using the Lyapunov stability theorem [28]. The selected Lyapunov function is

$$V_1(X) = X_1^T P_1 X_1 + \lambda_1 k_1^2, \quad \lambda_1 > 0 \quad (40)$$

where P_1 is the symmetrical positive definite matrix and the state variable $\mathbf{X}_1 = [x_1, x_2]^T = [e_1, \dot{e}_1]^T$.

Matrix P_1 can be deduced as follows

$$P_1 = \begin{bmatrix} 1.414 & 0.5 \\ 0.5 & 0.707 \end{bmatrix} \quad (41)$$

The adaptive law in the x_a-direction is

$$\dot{k}_{c1} = \frac{1}{\lambda_1 k_{p1}} X_1^T P_1 B_1 x_a^* = \frac{1}{\lambda_1 k_{p1}}(0.5e_1 + 0.707\dot{e}_1)x_a^* \quad (42)$$

(42) indicates that the adaptive law in the x_a-direction is determined by X_1, k_c, error e, and rate of change error $\dot{e}$; thus, the subsystem will have good stability and coincide with the MRA in real time. A reference controller is added to the subsystem according to the principle of adaptive control to enhance the robustness, stability and tracking performance. The transfer function of the reference controller is as follows

$$C_1(s) = F_1(s)G^{-1}(s) = \frac{s^2 + 1.414s + 1}{(2s + 1)^2} \quad (43)$$

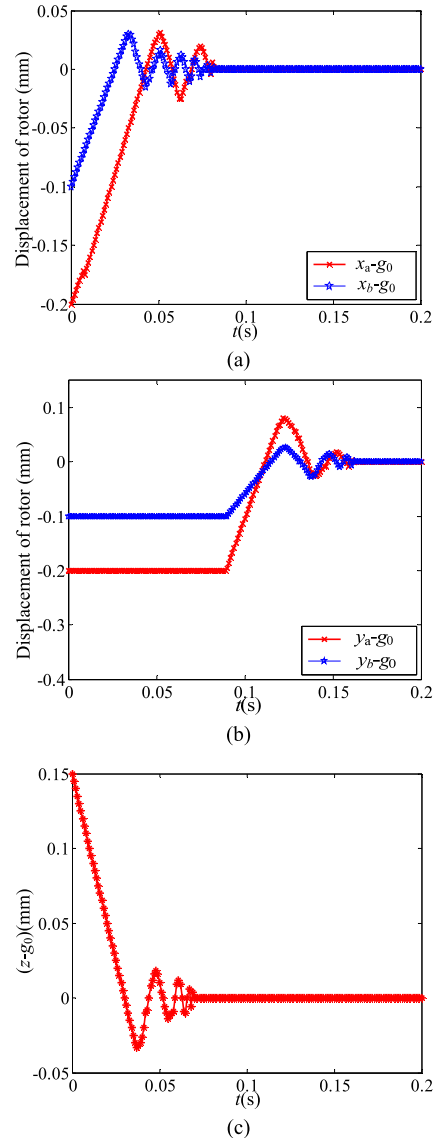where $F_1(s)$ is the second-order low-pass-filtered function.

FIGURE 10. Simulation using NNGI control scheme. (a) Displacements in x_a- and x_b-directions. (b) Displacements in y_a- and y_b-directions. (c) Displacements in z-direction.

TABLE 2. Parameters of the PID controller.

Parameter	Value	Parameter	Value
k_p	5	T_l	0.02 s
T_d	0.003 s		

The design processes of the other four adaptive laws are similar. The adaptive laws in the other four directions are as follows

$$\dot{k}_{c2} = \frac{1}{\lambda_2 k_{p2}} X_2^T P_2 B_2 x_b^* = \frac{1}{\lambda_2 k_{p2}}(0.5e_2 + 0.707\dot{e}_2)x_b^* \quad (44)$$

$$\dot{k}_{c3} = \frac{1}{\lambda_3 k_{p3}} X_3^T P_3 B_3 y_a^* = \frac{1}{\lambda_3 k_{p3}}(0.5e_3 + 0.707\dot{e}_3)y_a^* \quad (45)$$
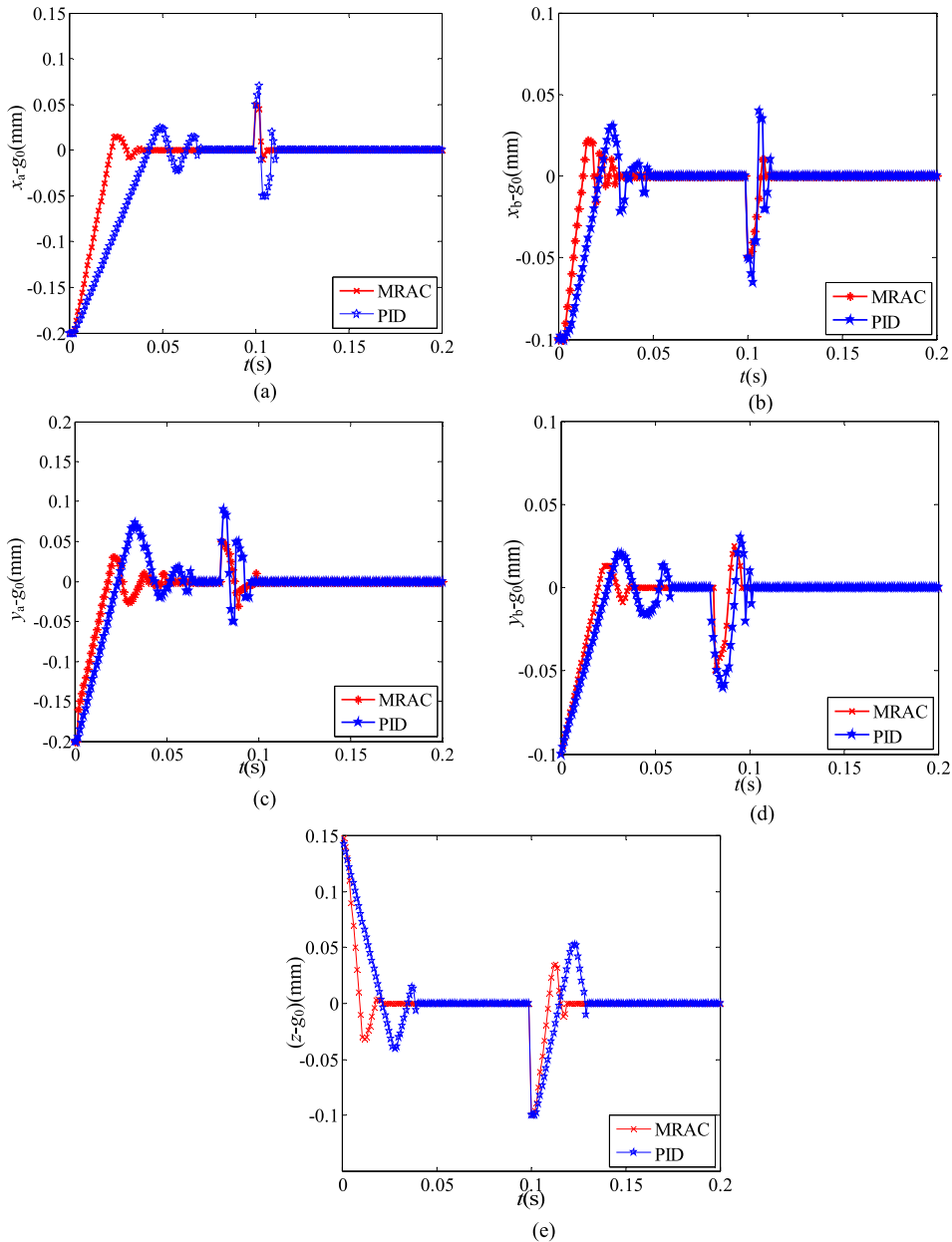
FIGURE 11. Simulated responses for the MRA-NNGI and PID-NNGI control strategies. (a) Displacements in the x_a-direction for the two different control methods. (b) Displacements in the x_b-direction for the two different control methods. (c) Displacements in the y_a-direction for the two different control methods. (d) Displacements in the y_b-direction for the two different control methods. (e) Displacements in the z-direction for the two different control methods.

$$\dot{k}_{c4} = \frac{1}{\lambda_4 k_{p4}} X_4^T P_4 B_4 y_b^* = \frac{1}{\lambda_4 k_{p4}}(0.5e_4 + 0.707\dot{e}_4)y_b^* \tag{46}$$

$$\dot{k}_{c5} = \frac{1}{\lambda_5 k_{p5}} X_5^T P_5 B_5 z^* = \frac{1}{\lambda_5 k_{p5}}(0.5e_5 + 0.707\dot{e}_5)z^* \tag{47}$$

V. VALIDATION

First, comparative simulations are conducted using MATLAB to verif *y* the validity and superiority of the 5-DOF wind turbine system with the NNGI control scheme and MRA controllers. Then, startup and anti-jamming experiments are carried out to validate the decoupling performance of MRA-NNGI based on a TMS320F2821 DSP and a control computer. The parameters of the 5-DOF rigid rotor system are given in Table 1, and the power amplification factor is set at $k_s = 20000$. The air gap width at the equilibrium position is set at $g_0 = 1$ mm, the initial gap lengths in five directions are set at $x_a = y_a = 0.8$ mm, $x_b = y_b = 0.9$ mm and $z = 1.15$ mm, and the rotor speed is set at 250 r/min.

A. DECOUPLING PROPERTIES OF NNGI CONTROL SCHEME

To demonstrate the decoupling properties of the NNGI control scheme, simulations of the displacements of the rotor in 5 directions are carried out. As shown in Fig. 10(a), the initial displacements in the x_a- and x_b-directions are -0.2 mm and -0.1 mm, respectively. When the displacements are from the initial values to 0 mm at $t = 0$ s, as for the NNGI control scheme, the rotor returns to equilibrium in the x_a- and x_b-directions after a period of overshoots, and the displacements in other directions are almost unchanged.

Fig. 10(b) depicts the displacements of the rotor in the y_a- and y_b-directions. When the displacements are from the initial values to 0 mm at $t = 0.1$ s, there are almost no fluctuations of the displacements of the rotor in the x_a- and x_b-directions. Fig. 10(c) shows that the displacement of the rotor in the z-direction is from an initial value to 0 mm at $t = 0$ s; the displacements in the other directions have almost no fluctuations. It is clear that the rotor system with the NNGI control scheme can be well decoupled.

B. COMPARISON WITH MRA-NNGI AND PID-NNGI

Two methods, namely, 1) the proposed control scheme (MRA-NNGI) and 2) the conventional PID control scheme (PID-NNGI), are used in this study to verify the decoupling, tracking, disturbance and robustness properties. The parameters of the PID controller are given in Table 2, and the displacement curves in the x_a-, y_a-, x_b-, y_b- and z- directions are shown in Fig. 11.

Fig. 11(a) presents the comparison of the two methods in the x_a-direction. When the displacement in the x_a-direction is from the initial values to 0 mm at $t = 0$ s, the system with the MRA-NNGI control scheme is stabilized at approximately $t = 0.052$ s, whereas the system with the PID controller is stabilized at approximately $t = 0.071$ s. As shown by the other figures in Fig. 11, the durations of stability of the MRA-NNGI for 5-DOF are shorter than those of the PID-NNGI.

Fig. 11 also presents a comparison between the two methods under the influence of disturbances. Taking Fig. 11(b) for example, the system with the MRA-NNGI control scheme is stabilized at approximately $t = 0.113$ s when the disturbance is added at $t = 0.1$ s, and the system with the PID controller is stabilized at approximately $t = 0.123$ s. The same can be concluded based on several other simulation diagrams. Thus, the tracking properties of the proposed control scheme (MRA-NNGI) are superior to those of the traditional PID control scheme (PID-NNGI).

Fig. 11 shows that when the disturbance is imposed in the radial x-direction at $t = 0.1$ s, the deviations in the y-direction when the MRA-NNGI control scheme is used are almost not influenced. The decoupling properties of the NNGI control scheme for this system are good. The displacements of the rotor in the x_a- and x_b-directions are almost unchanged when the disturbance is added in the

y_a- and y_b-directions at $t = 0.08$ s. The momentary overshoots and the recovery time of the PID-NNGI are greater than those of the MRA-NNGI when the disturbance is imposed. It can also be seen from Fig. 11 that there is little influence on the rotor in the radial direction when the disturbance is added in the z-direction. Therefore, the decoupling, tracking, disturbance, and robustness properties of the MRA-NNGI are superior to those of the PID-NNGI.
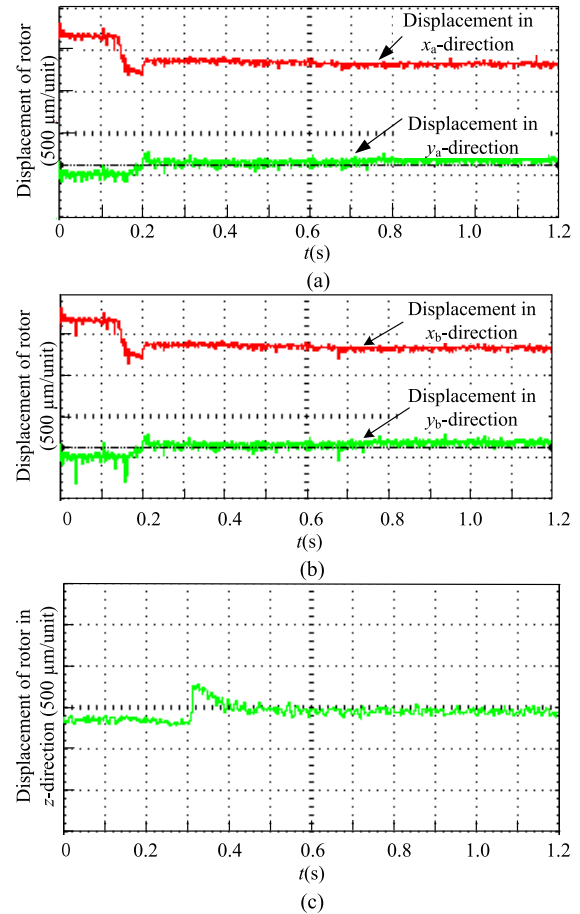
FIGURE 12. Startup displacement curves of rotor. (a) Displacement of rotor in x_a- and y_a-directions. (b) Displacement of rotor in x_b- and y_b-directions. (c) Displacement of rotor in z-direction.

C. EXPERIMENTAL VALIDATIONS

To verify the decoupling effectiveness of the MRA-NNGI control, startup and anti-jamming experiments are carried out on the prototype. Five displacement sensors are used to detect the displacements of the rotor in 5 directions, and the startup displacement curves of the rotor are shown in Fig. 12. The radial displacements in the x_a-, y_a-, x_b-, and y_b-directions are shown in Fig. 12(a) and (b), and the displacement in the z-direction is shown in Fig. 12(c). From Fig. 12, when using the MRA-NNGI control scheme, the rotor is pulled back to the radial equilibrium position from the initial position at approximately $t = 0.21$ s when the radial levitation currents are loaded in the levitation windings at $t = 0.14$ s. In addition,

the rotor is pulled back to the equilibrium position in the z-direction at approximately $t = 0.4$ s when the axial control current is loaded at $t = 0.3$ s. As shown in Fig. 12, using the MRA-NNGI control, there is little influence in the 5 directions.
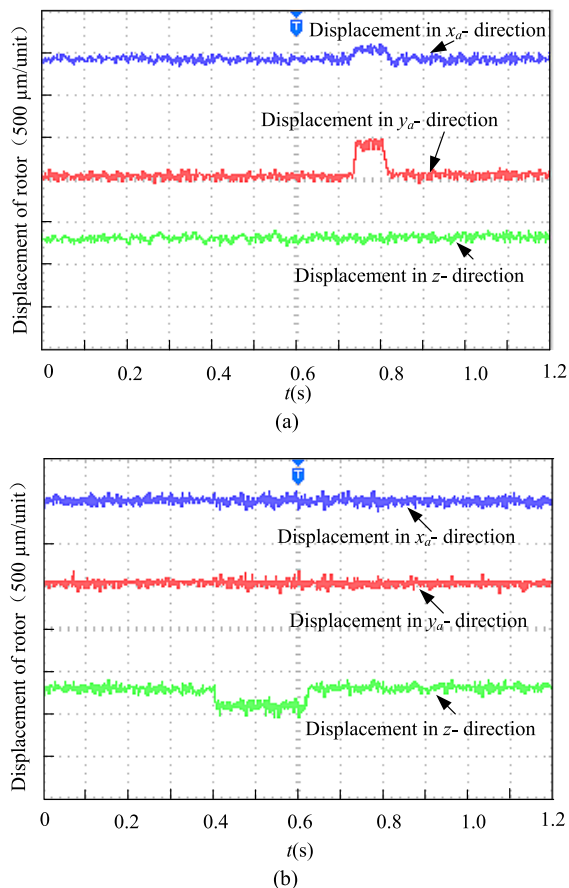

FIGURE 13. Displacement curves of rotor under disturbances.
(a) Displacement of rotor when the disturbance is added in the radial direction. (b) Displacement of rotor under a disturbance in the z-direction.

To verify the dynamic stability of the rotor system, external disturbances are applied to the rotor in the x_a-, y_a- and z-directions when the rotor of the wind turbine is operating at the rated speed. From Fig. 13(a), it can be seen that the displacement in the z-direction is almost unchanged when the disturbances are added in the radial x_a- and y_a-directions. It can also be seen from Fig. 13(b) that the radial displacements are almost unchanged when the disturbance is added in the z-direction at $t = 0.4$ s.

Thus, the results of the simulations and experiments reveal that the proposed control scheme, which combines the NNGI control scheme and MRA controllers, has exceptional decoupling, robustness and stability.
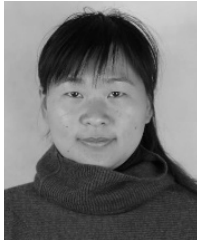
VI. CONCLUSIONS

A new MRA-based NNGI scheme for decoupling control of a 5-DOF rotor system is proposed in this study with consideration of the strong coupling, multivariable and nonlinear nature

of a 5-DOF rotor system. The simulations and experiments demonstrate the following: 1) after putting five NNGI systems in front of the original system, a simple open-loop generalized pseudo-linear system is achieved, and the 5-DOF rotor system is decoupled; 2) the dynamic, anti-disturbance, and decoupling performances can be effectively improved using the MRA controllers based on the NNGI control scheme.
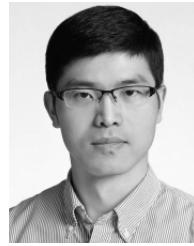
REFERENCES

[1] J. Njiri and D. Söffker, "State-of-the-art in wind turbine control: Trends and challenges," *Renew. Sustain. Energy Rev.*, vol. 60, pp. 377–393, Jul. 2016.

[2] T. Göçmen, P. van der Laan, P.-E. Réthoré, A. P. Diaz, and G. C. Larsen, "Wind turbine wake models developed at the Technical University of Denmark: A review," *Renew. Sustain. Energy Rev.*, vol. 60, pp. 752–769, Jul. 2016.

[3] J. Wang, R. Qu, T. Tang, and Y. Liu, "Design of a superconducting synchronous generator with LTS field windings for 12 MW offshore direct-drive wind turbines," *IEEE Trans. Ind. Electron.*, vol. 63, no. 3, pp. 1618–1628, Mar. 2016.

[4] W. Jun, Y. Peng, and W. Qiao, "Current-aided order tracking of vibration signals for bearing fault diagnosis of direct-drive wind turbines," *IEEE Trans. Ind. Electron.*, vol. 63, no. 10, pp. 6336–6346, Oct. 2016.

[5] B. Han, Q. Xu, and Q. Yuan, "Multiobjective optimization of a combined radial-axial magnetic bearing for magnetically suspended compressor," *IEEE Tran. Ind. Electron.*, vol. 63, no. 4, pp. 2284–2293, Apr. 2016.

[6] H. Mitterhofer, W. Gruber, and W. Amrhein, "On the high speed capacity of bearingless drives," *IEEE Trans. Ind. Electron.*, vol. 61, no. 6, pp. 3126–3131, Jun. 2014.

[7] H. Zhu, S. Ding, and J. Jv, "Modeling for three-pole radial hybrid magnetic bearing considering edge effect," *Energies*, vol. 9, no. 5, p. 345, May 2016.

[8] J. Kumbernuss, C. Jian, J. Wang, H. X. Yang, and W. N. Fu, "A novel magnetic levitated bearing system for vertical axis wind turbines (VAWT)," *Appl. Energy*, vol. 90, no. 1, pp. 148–153, Feb. 2012.

[9] X. Sun, L. Chen, and Z. Yang, "Overview of bearingless permanent magnet synchronous motors," *IEEE Trans. Ind. Electron.*, vol. 60, no. 12, pp. 5528–5538, Dec. 2013.

[10] M. Jang, C. Chen, and Y. Tsao, "Sliding mode control for active magnetic bearing system with flexible rotor," *J. Franklin Inst.*, vol. 342, no. 4, pp. 401–419, Jul. 2005.

[11] L. Gentili and L. Marconi, "Robust nonlinear disturbance suppression of a magnetic levitation system," *Automatica*, vol. 39, no. 4, pp. 735–742, Apr. 2003.

[12] S. Sivrioglu and K. Nonami, "Adaptive output backstepping control of a flywheel zero-bias AMB system with parameter uncertainty," in *Proc. 42nd Decision Control*, 2003, pp. 3942–3947.

[13] J. Cao and Q. Chen, "Decoupling control for a 5-DOF rotor supported by active magnetic bearings," in *Proc. 6th Electr. Mach. Syst.*, Beijing, China, 2003, pp. 477–480.

[14] W. Tong and F. Jiancheng, "A feedback linearization control for the nonlinear 5-DOF flywheel suspended by the permanent magnet biased hybrid magnetic bearings," *Acta Astron.*, vol. 79, pp. 131–139, Oct./Nov. 2012.

[15] X. Sun, L. Chen, H. Jiang, Z. Yang, J. Chen, and W. Zhang, "High-performance control for a bearingless permanent-magnet synchronous motor using neural network inverse scheme plus internal model controllers," *IEEE Trans. Ind. Electron.*, vol. 63, no. 6, pp. 3479–3488, Jun. 2016.

[16] S. Ahmed and K. Mohamed, "Neural-network-based speed controller for induction motors using inverse dynamics model," *Eur. Phys. J. Plus*, vol. 131, pp. 292–303, Aug. 2016.

[17] S. Naji *et al.*, "Estimating building energy consumption using extreme learning machine method," *Energy*, vol. 97, pp. 506–516, Feb. 2016.

[18] X. Sun, Z. Shi, L. Chen, and Z. Yang, "Internal model control for a bearingless permanent magnet synchronous motor based on inverse system method," *IEEE Trans. Energy Convers.*, vol. 31, no. 4, pp. 1539–1548, Dec. 2016.

[19] G. Liu, L. Chen, W. Zhao, and Y. Jiang, "Internal model control of permanent magnet synchronous motor using support vector machine generalized inverse," *IEEE Trans. Ind. Informat.*, vol. 2, no. 2, pp. 890–898, May 2013.

[20] J. B. Hoagg, and D. S. Bernstein, "Retrospective cost model reference adaptive control for nonminimum-phase discrete-time systems, Part 1: The adaptive controller," in *Proc. 49th Decision Control*, Atlanta, CA, USA, 2010, pp. 2933–2938.

[21] X. Sun, L. Chen, Z. Yang, and H. Zhu, "Speed-sensorless vector control of a bearingless induction motor with artificial neural network inverse speed observer," *IEEE/ASME Trans. Mechatronics*, vol. 18, no. 4, pp. 1357–1366, Aug. 2013.

[22] A. Ben-Israel and T. Greville, *Generalized Inverses: Theory and Applications*, 2nd ed. New York, NY, USA: Springer, 2003.

[23] H. Zhang, Y. Kun, G. Liu, D. Hu, and W. Zhao, "Fuzzy self-tuning decoupling control based on neural network of three-motor drive system," *Control Theory Appl.*, vol. 30, no. 9, pp. 1178–1186, Sep. 2013.

[24] W. Sun, Y. Zhang, Y. Huang, H. Gao, and O. Kaynak, "Transient-performance-guaranteed robust adaptive control and its application to precision motion control systems," *IEEE Trans. Ind. Electron.*, vol. 63, no. 10, pp. 6510–6518, Oct. 2016.

[25] K. H. Kim, "Model reference adaptive control based adaptive current control scheme of a PM synchronous motor with an inproved servo performance," *IET Electr. Power Appl.*, vol. 3, no. 1, pp. 8–18, Jan. 2009.

[26] Y. Yu, H. Zhu, and S. Zeng, "A new self-decoupling magnetic levitation generator for wind turbines," *Progr. Electromagn. Res. M*, vol. 40, pp. 111–118, Jan. 2014.

[27] X. Sun, B. Su, L. Chen, Z. Yang, X. Xu, and Z. Shi, "Precise control of a four degree-of-freedom permanent magnet biased active magnetic bearing system in a magnetically suspended direct-driven spindle using neural network inverse scheme," *Mech. Syst. Signal Process.*, vol. 88, pp. 36–48, May 2017.

[28] I. Ranatunga, F. L. Lewis, O. P. Dan, and S. M. Tousif, "Adaptive admittance control for human-robot interaction using model reference design and adaptive inverse filtering," *IEEE Trans. Control Syst. Technol.*, vol. 25, no. 1, pp. 278–285, Jan. 2017.

XIAODONG SUN (M'12) received the B.Sc. degree in electrical engineering and the M.Sc. and Ph.D. degrees in control engineering from Jiangsu University, Zhenjiang, China, in 2004, 2008, and 2011, respectively.

Since 2004, he has been with Jiangsu University, where he is currently a Professor with the Automotive Engineering Research Institute. From 2014 to 2015, he was a Visiting Scholar with the School of Electrical, Mechanical, and Mechatronic Systems, University of Technology Sydney, Sydney, Australia. His areas of interest include electrical machines and drives, drives and control for electric vehicles, and intelligent control.

YANJUN YU received the B.Sc. degree in electrical engineering and M.Sc degree in power electronics and power transmission from Jiangsu University, Zhenjiang, China, in 2004 and 2009, respectively. She is currently pursuing the Ph.D. degree with the School of Electrical Information Engineering, Jiangsu University.

Her current research interests include structure parameter design, analysis, and control technology for magnetic bearings and wind turbines.

WEIYU ZHANG received the B.Sc. degree in control engineering and the Ph.D. degree in electrical engineering from Jiangsu University, Zhenjiang, China, in 2009 and 2014, respectively. Since 2014, she has been with the School of Electrical and Information Engineering, Jiangsu University, where she is currently a Lecturer. Her research interests include structure parameter design and control technology for magnetic bearings.

• • •